

High T_c via spin fluctuations from incipient bands: application to monolayers and intercalates of FeSe

A. Linscheid,¹ S. Maiti,¹ Y. Wang,² S. Johnston,² and P. J. Hirschfeld¹

¹*Department of Physics, University of Florida, Gainesville, FL 32611*

²*Department of Physics and Astronomy, University of Tennessee, Knoxville, Tennessee 37996*

(Dated: March 14, 2016)

We investigate superconductivity in a two-band system with an electron- and hole-like band, where one of the bands is away from the Fermi level (or “incipient”). We argue that the incipient band contributes significantly to spin-fluctuation pairing in the strong coupling limit where the system is close to a magnetic instability, and can lead to a large T_c . In this case, T_c is limited by a competition between the frequency range of the coupling (set by an isolated paramagnon) and the coupling strength itself, such that a dome-like T_c dependence on the incipient band position is obtained. The coupling of electrons to phonons is found to further enhance T_c . The results are discussed in the context of experiments on monolayers and intercalates of FeSe.

Introduction — Iron based superconductors (FeSC) form the largest family of unconventional superconductors (SC) known to us. This includes the stoichiometric, pressurized, doped and/or intercalated versions of quasi-2D layered Fe-pnictogen or Fe-chalcogen compounds of the 1111, 111, 122, and 11 families. These systems collectively host a variety of superconducting phases and exhibit a broad range T_c 's [1–4], which still lack a consistent explanation. Among these, the FeSe systems present a curious phenomenology: almost all members related to this family –alkali/alkali-hydroxy intercalated FeSe [5–7], ammonia intercalated FeSe [8–11]– exhibit $T_c \sim 35$ –45 K and even reaching 60–70 K in the case of single unit cell (UC) thick FeSe grown on 001-SrTiO₃ (STO) [12–15], 110-STO, and [16, 17] 001-BaTiO₃ (BTO) [18]. Even bulk FeSe, which has a T_c of only 8 K [19], exhibits a maximum T_c of 36 K [20] under pressure.

Thus far, the relatively high T_c 's in these systems have been correlated with an increase of the *ab*-plane lattice constant in multi UC FeSe films [21, 22] or an increase in the *c*-axis lattice constant in the intercalates [22]. The evolution from single- to multi-UC films is not smooth [23], but the general trend is that T_c is suppressed when more layers are added. Another correlation, particular to the 1 UC FeSe on STO (and BTO), is based on the observation of ‘replica’ bands ~ 100 meV below the electron and hole bands [15]. This is indicative of a strong forward-focussed ($\mathbf{q} = 0$) electron-phonon (e-ph) coupling to a polar phonon mode of the doped STO substrate, which was recently invoked to explain the high T_c of the interfaces [15, 24–26].

This, however, does not explain the relatively high T_c in the other FeSe systems without STO phonons, nor why electron doping the FeSC and removing the hole Fermi pockets seems generally to enhance T_c [2, 27]. This empirical trend also appears to directly contradict the spin fluctuation pairing scenario for FeSC, where the pair scattering by repulsive interactions between hole and electron Fermi pockets (separated by \mathbf{Q}) leads to strong pairing;

naively, removing the hole pocket should destroy this interaction and suppress T_c rapidly. Indeed, while a recent work on incipient band pairing showed that if pairing exists making use of electronic states at the Fermi level, superconductivity can also be induced in incipient bands [28], the authors also found that moving the hole band away from the Fermi level always suppresses T_c within the weak coupling framework.

We address these issues in this Letter by noting that an interesting, and often overlooked, clue lies in the electronic structure of FeSe systems. Although all the FeSe systems have electron-like Fermi pockets at the *M*-points, another common aspect is that they have an incipient hole band 50–100 meV below the Fermi level [5, 12–15]. This incipient hole band, neglected in nearly all analyses of SC pairing, is shown here to play a crucial role in the strong coupling regime.

Since the FeSe systems are generally tetragonal and quasi-2D, it suffices to consider a rather simple model of their electronic structure. Here, we adopt a two band system with a regular electron band and incipient hole band. We then solve Eliashberg-type equations in which the pairing glue is provided by the interband spin-fluctuations (SF), considered in the strong coupling regime close to a magnetic instability. We argue that the FeSe systems are able to sustain stronger electronic correlations without developing magnetic long range order due to the suppression of interband scattering by the incipient electronic states.

The proximity to magnetism is well established in these systems. In fact, the interpretation of the data in Refs. [21] and [27] suggests that FeSe film thickness as low as 3 UC on STO results in a hole band crossing the Fermi level, which is accompanied by spectral features associated with a magnetic state, while a large T_c is recovered in such thicker films by electron doping [27]. Further, a first principles study [29] of 1 UC FeSe/STO found that FeSe would have a very strong spin-density wave (SDW) without the substrate induced electron doping, again sug-

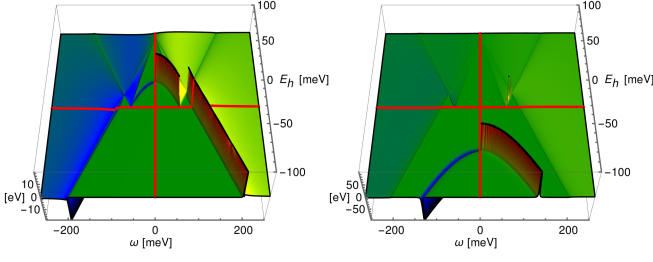


Figure 1. (color online) Imaginary part of $V^{\text{SF}}(\mathbf{Q}, \omega + i\eta)$ for $U = 0.325\text{eV}$ (left) and $U = 0.5\text{eV}$ (right) for a range of E_h . The Lifshitz transition $E_h = 0$ and the zero energy line $\omega = 0$ are highlighted in red.

gesting strong correlations in the system.

Accounting for the close proximity to magnetic order and strong correlations allowed for by the incipient band, we find that the pairing is dominated by a sharp paramagnon peak in the SF propagator at an energy Ω_p that is induced near energies corresponding to the onset of interband transitions. Due to the electronic origin of the bosonic peak, its position controls both the pairing bandwidth and the coupling strength (unlike a phonon mechanism where the two are largely independent). As the peak hardens, the interplay between the above two quantities results in a non-monotonic behavior of T_c . Introducing an additional e-ph coupling further enhances T_c , as was pointed out in Ref. [28]. We now present the systematics of our result.

Model — We take the electron and hole band dispersions as ($\hbar = 1$)

$$\varepsilon_{\mathbf{k}}^h = -\frac{\mathbf{k}^2}{2m_h^*} + E_h, \quad \varepsilon_{\mathbf{k}}^e = \frac{(\mathbf{k} - \mathbf{Q})^2}{2m_e^*} + E_e, \quad (1)$$

where m_e^* (m_h^*) is the effective electron (hole) band mass, E_e (E_h) is the electron (hole) band extrema measured relative to the chemical potential μ , and \mathbf{Q} is the wave-vector at which SFs are peaked. The bandwidth is set by requiring the bands to extend up to Λ_B around their respective centers in momentum space. We convert all momenta in our plots to energy using m_h^* . In all numerical plots we fix $\Lambda_B = 900$ meV and $E_e = -60$ meV, unless otherwise specified.

In the spin fluctuation framework, the bosonic propagator providing the pairing glue is the transverse interband spin susceptibility $\chi_{\text{he}}^{\uparrow\downarrow}(\mathbf{q}, i\nu_n)$ (we shall henceforth drop the spin indices). Under the usual FLEX-based approximations [30–33], the susceptibility acquires a Stoner-like enhancement and the propagator can be modeled as

$$V^{\text{SF}}(\mathbf{q}, i\nu_n) = \frac{U^2 (\chi_{\text{he}}^0(\mathbf{q}, i\nu_n) + \chi_{\text{eh}}^0(\mathbf{q}, i\nu_n))}{1 - U (\chi_{\text{he}}^0(\mathbf{q}, i\nu_n) + \chi_{\text{eh}}^0(\mathbf{q}, i\nu_n))}, \quad \text{where} \\ \chi_{\text{he}}^0(\mathbf{q}, i\nu_n) = - \int \frac{d^2\mathbf{k}}{4\pi^2} \frac{f(\varepsilon_{\mathbf{k}}^h) - f(\varepsilon_{\mathbf{k}+\mathbf{q}}^e)}{i\nu_n + \varepsilon_{\mathbf{k}}^h - \varepsilon_{\mathbf{k}+\mathbf{q}}^e} = \chi_{\text{eh}}^0(\mathbf{q}, -i\nu_n). \quad (2)$$

Here, f is the Fermi function and $U > 0$ is a repulsive point-contact interaction parameter that has the same scale as those in Hubbard-Hund type models [31, 32]. Note that we are discarding the remaining charge and spin susceptibilities that arise in the FLEX formalism. We therefore expect to overestimate T_c in this approach.

In the weak coupling limit ($u \equiv m_e^* m_h^* U / 2\pi(m_e^* + m_h^*) \ll 1$), for the incipient case ($E_h < 0$), the propagator V^{SF} is nonsingular and can be treated as a constant [28]. For $u \sim 1$, however, the system hosts a sharp paramagnon peak (a pole at $\Omega = \Omega_p$ in the retarded V^{SF}) controlled by E_h . (see Fig. 1). The position of this peak determines not only the size of the electron-SF coupling but also the ‘pairing bandwidth’ Λ_{SF} over which the pairing interaction acts.

An estimate for T_c — Before we analyze the solutions to the Eliashberg equations we offer a qualitative picture of the interplay between the coupling and the pairing bandwidth Λ_{SF} . To proceed, we focus on $\mathbf{q} = \mathbf{Q}$; it will be shown later that for the incipient case ($E_h < 0$), the \mathbf{q} dependence of V^{SF} near \mathbf{Q} is relatively weak. Then, for $E_h < 0$, $\Lambda_B \gg E_{h,e}$ and $T = 0$, we obtain

$$\chi_{\text{he}}^0(\mathbf{Q}, \Omega_p) = -\frac{m_e^*}{2\pi(r+1)} \ln\left[\frac{r|E_e| + |E_h| + \Omega_p}{\Lambda_B(1+r)}\right], \quad (3)$$

where $r = m_e^*/m_h^*$. It is clear from Eq. (2) that a magnetic instability sets in for $U = U_c \equiv 1/[\chi_{\text{he}}^0(\mathbf{Q}, 0) + \chi_{\text{eh}}^0(\mathbf{Q}, 0)]$. For $U < U_c$, we have a paramagnon peak at

$$\Omega_p^2 = (|E_h| + r|E_e|)^2 - E_0^2 \rightarrow 2E_0(E_h^* - E_h) \quad (4)$$

as the instability is approached, where the paramagnon softens at $E_h = E_h^* \equiv -E_0 + r|E_e|$ and $E_0 \equiv \Lambda_B(1+r)e^{-\frac{1}{2u}}$.

In the usual BCS picture, the dimensionless electron-boson coupling v_{SF} is obtained from the static limit of the propagator multiplied by density of states and the bandwidth of the pairing interaction Λ_{SF} is approximately the position of the bosonic mode Ω_p . Thus,

$$V_{\text{SF}}^{\text{stat}}(\mathbf{Q}) = U \frac{uR}{1 - uR} \rightarrow U \frac{E_0}{|E_h - E_h^*|}, \quad (5)$$

with $R = -2 \ln[|rE_e + E_h|/\Lambda_B(1+r)]$ and $v_{\text{SF}}^{e/h} = V_{\text{SF}}^{\text{stat}} m_{e/h}^*/2\pi$. To get an estimate for T_c , we note that as a function of E_h , the coupling v_{SF} varies from $v_{\text{SF}} \gg 1$ near E_h^* to $v_{\text{SF}} \ll 1$ far from E_h^* (see Fig. 2a). For $v_{\text{SF}} \ll 1$, T_c is given by $\Lambda_{\text{SF}} \exp[-1/v_{\text{SF}}^2]$; for $v_{\text{SF}} \gg 1$, T_c has the usual Allen-Dynes [34] lower bound given by $\Lambda_{\text{SF}}(v_{\text{SF}}^e v_{\text{SF}}^h)^{1/4}$. Near the instability, the coupling v_{SF} diverges as $1/|E_h - E_h^*|$ and the pairing bandwidth Λ_{SF} vanishes as $\sqrt{|E_h - E_h^*|}$ (as is clear from Eqs. 4 and 5), and the lower bound

$$T_c \gtrsim E_0 \left(\frac{m_e^* + m_h^*}{\sqrt{m_e^* m_h^*}} \right)^{1/2} \quad (6)$$

is then obtained for T_c .

If the coupling constant diverges, it is tempting to conclude that $T_c \rightarrow \infty$ within Eliashberg theory. However, we have demonstrated that even within an Eliashberg type theory, the T_c remains finite. This is a hallmark of a strong coupling electronic mechanism for superconductivity. The schematic evolution of T_c with E_h based on these considerations is presented in Fig. 2b. The suppression of T_c near E_h^* is a consequence of the dynamics of the pairing interaction, which leads to a strong mass renormalization of quasiparticles in the Fermi-liquid state. This aspect is not present in conventional e-ph theories because the coupling and the boson frequency are usually decoupled.

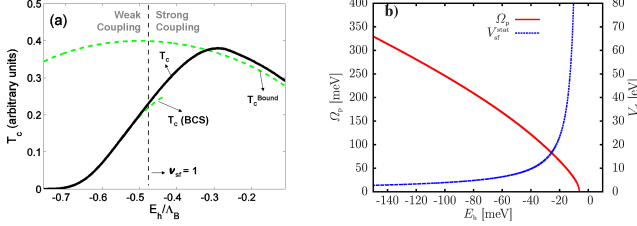


Figure 2. (Color online) a) Schematic of T_c as E_h is varied. T_c interpolates between the BCS behavior in the weak coupling regime ($v_{\text{SF}} \ll 1$) and the strong coupling lower bound for $v_{\text{SF}} \gg 1$. b) The paramagnon and the static propagator $V_{\text{SF}}^{\text{stat}}$ ($U = 0.45$ eV). Here $m_e^* = 2.6m_e$ and $m_h^* = 1.6m_e$.

Incipient Eliashberg equations — To accurately describe the region close to the instability E_h^* , we need to turn to a description in terms of the Eliashberg equations. These can be greatly simplified if the effective interaction V^{SF} does not depend strongly on momentum transfer \mathbf{q} . In Fig. 3 we investigate this dependence around \mathbf{Q} , defining $\tilde{\mathbf{q}} = \mathbf{Q} + \mathbf{q}$. The Stoner-like enhancement leads to a

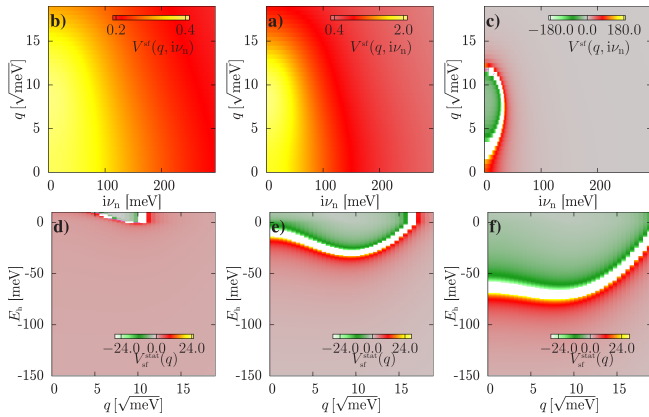


Figure 3. (color online) Momentum dependence of $V^{\text{SF}}(\mathbf{q}, i\nu_n)$ at $E_h = -65$ meV for $U = 0.4, 0.45$ and 0.51 eV in a), b) and c) and of the static part $V_{\text{SF}}^{\text{stat}}(\mathbf{q})$ for $U = 0.4, 0.45$ and 0.51 eV in d), e) and f) as a function Matsubara frequency and doping E_h , respectively. q measures the deviation from \mathbf{Q} .

strong variation of $V^{\text{SF}}(\mathbf{q}, i\nu_n = 0)$ close to the instability, as can be seen in Figs. 3a) - 3c). In Fig. 3d), 3e) and 3f) we show $V^{\text{SF}}(\mathbf{q}, 0)$ as a function of E_h and the momentum deviation q for the interaction parameters $U = 0.4, 0.45$, and 0.51 eV, respectively. The regions shown in green are beyond the instability and correspond to a magnetic ground state. Thus, in Fig. 3c), the magnetic instability occurs at a finite q leading to an incommensurate SDW ground state. As is evident in Fig. 3, the momentum dependence is only important very close to the instability and is rather featureless when the hole band goes deeper below the Fermi level; we conclude that the momentum dependence can be neglected in the Eliashberg equations in this region of parameter space.

The multiband isotropic Eliashberg equations in Matsubara axis are (see Supplemental information):

$$Z_{n,i} = 1 + \frac{T}{\omega_n} \sum_{n',i'} [\lambda_{n-n';i,i'}^{\text{ph}} \xi_{n',i'}^{\text{ph}} + \lambda_{n-n';i,i'}^{\text{SF}} \xi_{n',i'}^{\text{SF}}] \omega_{n'}$$

$$Z_{n,i} \Delta_{n,i} = T \sum_{n',i'} [\lambda_{n-n';i,i'}^{\text{ph}} \xi_{n',i'}^{\text{ph}} - \lambda_{n-n';i,i'}^{\text{SF}} \xi_{n',i'}^{\text{SF}}] \Delta_{n',i'}.$$

Here, $i, i' \in \{h, e\}$; $\xi_{n,i}^{\text{P}} = \int_{l_P}^{h_P} d\varepsilon / D_{n,i}$, with $D_{n,i} = \varepsilon^2 + Z_{n,i}^2 (\omega_n^2 + |\Delta_{n,i}|^2)$ and l_P, h_P being the cut-offs set by the mechanism $\text{P} \in \{\text{ph}, \text{SF}\}$ (the bandwidth in our calculations);

$\lambda_{n-n';i,i'}^{\text{SF}} = N_{i'} V^{\text{SF}}(\mathbf{Q}, i\omega_n - i\omega_{n'}) \delta_{i,i'}$, where $N_{h,e}$ are the density of states of the electron and hole bands; and $\lambda_{n-n';i,i'}^{\text{ph}} = \int d\Omega 2\Omega \alpha^2 F_{i,i'}(\Omega) / [(\omega_n - \omega_{n'})^2 + \Omega^2]$. We have neglected the single-particle energy renormalization $\chi_{n,i}$.

For the following numerical solution, we choose experimental parameters for FeSe on SrTiO₃ from Ref. [35]: $m_h^* = 1.6m_e$, $m_e^* = 2.6m_e$, lattice constant $a = 3.9$ Å, and $E_e = -60$ meV. In Fig. 4, we show the results from the numerical solution to the Eliashberg equations. Figure 4a), shows the gap value $\Delta(i\pi T)$ as a function of temperature and electron doping (E_h). For the given bandwidth $\Lambda_B = 900$ meV, we observe a maximum T_c at about the experimental position of the hole band ($E_h^{\text{exp}} = -78$ meV [35]) if we assume a reasonable interaction parameter of $U = 0.7$ eV.

In the panels 4d) and 4e), we show the temperature and doping dependence of the two \pm gaps, respectively. Note that the interband nature of the interaction makes the incipient hole gap larger than the electron band gap. This explains the counterintuitive trend in Fig. 4d) whereby the electron band gap is suppressed faster by continued electron doping while the hole band gap reaches its maximum at lower E_h .

In Fig. 4f), we plot the gap/ critical temperature ratio. For E_h far away from the instability, we find the BCS value of 3.5 for $2\Delta_e/T_c$, which increases as E_h moves towards the Fermi level to much larger values of about 9, reflecting the the strong coupling behavior near the magnetic instability. $2\Delta_h/T_c$ has a similar enhanced behavior

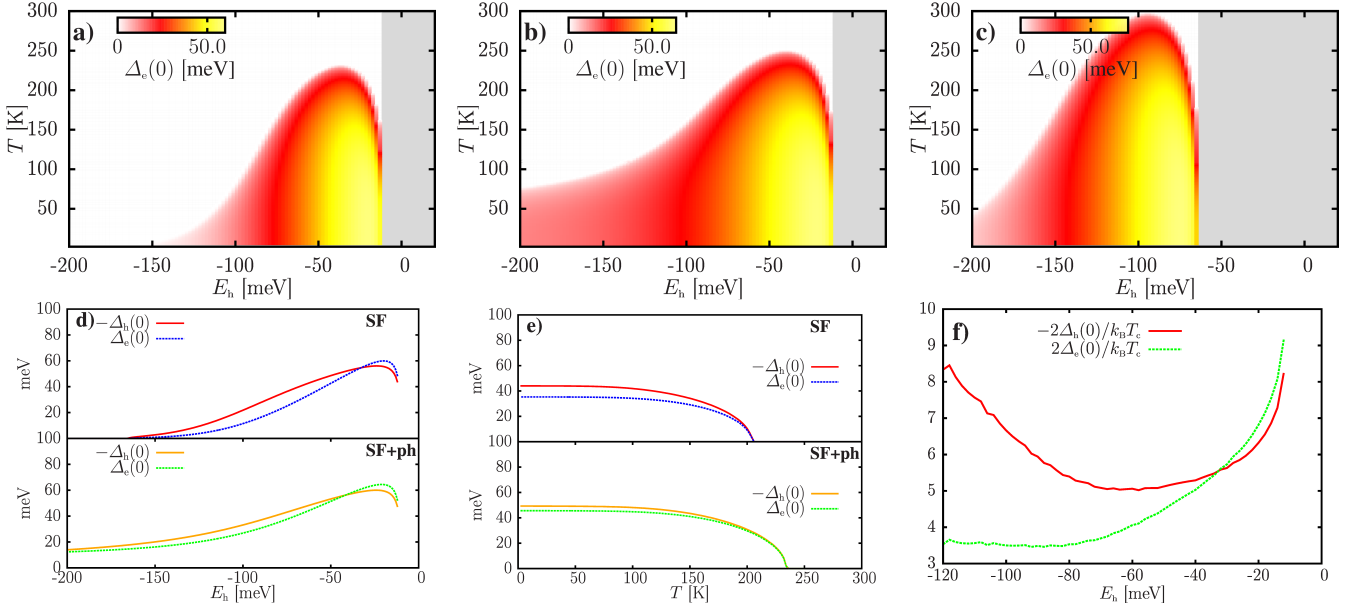


Figure 4. (color online) Gap on the electron band at the Fermi level as a function of doping (E_h) and temperature T in a) via spin fluctuations and in b) with an additional intraband phonon interaction of $\lambda_{ph} = 0.6$ and $\omega_{ph} = 100$ meV. Parameters are $U = 0.6$ eV and $\Lambda_B = 900$ meV. c) same as a) but with U increased to 0.7 eV. Shaded areas in a), b) and c) are antiferromagnetic. In d) we plot the two gaps as a function of doping at $T = 2$ K (top) and with the additional phonon interaction (bottom). e) SF gaps as a function of T (top) and with the additional phonon interaction (bottom) at $E_h = -60$ meV. f) Gap ratios for electron and hole gap vs. E_h .

close to the instability, but is also much larger than the electron band ratio far from the instability, as discussed in Ref. 28.

The overestimation of T_c — Our model produces possible T_c values well above 200 K. Note, however, that we have neglected the intra-band component of the repulsive interactions that will reduce this estimate. This is typically captured by the standard μ^* approximation; however, while one can easily show that an analogous RPA treatment leads to a Coulomb repulsion screened by the electron-band charge susceptibility, the use of the standard μ^* approximation is questionable due to the shallowness of the electron band. A more accurate calculation of this contribution requires momentum resolution, which would increase the complexity of our model. Thus, we leave this for future work. Finally, T_c is also likely to be suppressed in the real system due to increased fluctuations in 2D that are not captured by the Eliashberg formalism.

Role of phonons — Since the momentum dependence of the interactions is neglected here, we cannot account for the forward scattering nature of the e-ph interaction in the 1UC FeSe/STO. We note, however, that it will lead to a purely intraband phonon coupling. In this spirit, we add in Fig. 4b) an intra-band phonon interaction of with total coupling $\lambda_{ph} = 0.6$, $\Omega_{ph} = 100$ meV, and $\alpha^2 F_{i,i'}(\Omega) = \frac{\lambda_{ph} \Omega_{ph}}{2} \delta_{i,i'} \delta(\Omega - \Omega_{ph})$, which increases T_c^{\max} to 250 K at the optimal E_h and makes superconductivity persist to much lower E_h . We also note that the T_c

increase due to the phonons will likely be larger in a more accurate treatment of the forward scattering and/or the intraband repulsion. In the latter case there will a cancellation of the repulsive intraband interaction, that will make the influence of the attractive phonon interaction more prominent.

Conclusions — We have shown that when a magnetic instability nearly coincides with a band moving below the Fermi level, this so-called incipient band can play an important role in pairing. Within a simple two-band model, T_c in such a system was found to have a dome-like behavior due to the competition between the coupling strength and spin fluctuation bandwidth. Both of these are controlled by the paramagnon peak in the SF spectrum, which is present for systems with strong correlations ($u \sim 1$). For weakly correlated systems ($u \ll 1$), there is no such peak and one recovers the results of Ref [28]. With realistic values for the parameters, we find significant optimal values of T_c , even in the absence of Fermi surface-based interactions. In particular, for values relevant for FeSe/STO (we expect those of the intercalates to be similar), we find that the maximum T_c is clearly capable of explaining the high critical temperatures observed in these systems. Including an additional phonon coupling in the energy range of the suspected oxygen modes of STO observed in Ref. [15] further enhances the critical temperature.

Acknowledgements — The authors are grateful for useful discussions with T. Maier, V. Mishra, and D.J.

Scalapino. PJH and AL were supported by DE-FG02-05ER46236. S. J. and Y. W. are partially funded by the University of Tennessee's Science Alliance Joint Directed Research and Development (JDRD) program, a collaboration with Oak Ridge National Laboratory.

-
- [1] A. Chubukov and P. J. Hirschfeld, *Physics Today* **68**, 46 (2015).
 - [2] P. J. Hirschfeld, *Comptes Rendus Physique* **17**, 197 (2016).
 - [3] A. Chubukov, *Annual Review of Condensed Matter Physics* **3**, 57 (2012).
 - [4] H.-H. Wen and S. Li, *Annual Review of Condensed Matter Physics* **2**, 121 (2011).
 - [5] T. Qian, X.-P. Wang, W.-C. Jin, P. Zhang, P. Richard, G. Xu, X. Dai, Z. Fang, J.-G. Guo, X.-L. Chen, and H. Ding, *Physical review letters* **106**, 187001 (2011).
 - [6] X. H. Niu, R. Peng, H. C. Xu, Y. J. Yan, J. Jiang, D. F. Xu, T. L. Yu, Q. Song, Z. C. Huang, Y. X. Wang, B. P. Xie, X. F. Lu, N. Z. Wang, X. H. Chen, Z. Sun, and D. L. Feng, *Physical Review B* **92**, 060504 (2015).
 - [7] L. Zhao, A. Liang, D. Yuan, Y. Hu, D. Liu, J. Huang, S. He, B. Shen, Y. Xu, X. Liu, L. Yu, G. Liu, H. Zhou, Y. Huang, X. Dong, F. Zhou, K. Liu, Z. Lu, Z. Zhao, C. Chen, Z. Xu, and X. J. Zhou, *Nature Communications* **7**, 10608 (2016).
 - [8] J. Guo, H. Lei, F. Hayashi, and H. Hosono, *Nature communications* **5**, 4756 (2014).
 - [9] S. J. Sedlmaier, S. J. Cassidy, R. G. Morris, M. Drakopoulos, C. Reinhard, S. J. Moorhouse, D. O'Hare, P. Manuel, D. Khalyavin, and S. J. Clarke, *Journal of the American Chemical Society* **136**, 630 (2014).
 - [10] M. Burrard-Lucas, D. G. Free, S. J. Sedlmaier, J. D. Wright, S. J. Cassidy, Y. Hara, A. J. Corkett, T. Lancaster, P. J. Baker, S. J. Blundell, and S. J. Clarke, *Nature materials* **12**, 15 (2013).
 - [11] D. Guterding, H. O. Jeschke, P. J. Hirschfeld, and R. Valentí, *Physical Review B* **91**, 041112 (2015).
 - [12] Q.-Y. Wang, Z. Li, W.-H. Zhang, Z.-C. Zhang, J.-S. Zhang, W. Li, H. Ding, Y.-B. Ou, P. Deng, K. Chang, J. Wen, C.-L. Song, K. He, J.-F. Jia, S.-H. Ji, Y.-Y. Wang, L.-L. Wang, X. Chen, X.-C. Ma, and Q.-K. Xue, *Chinese Physics Letters* **29**, 037402 (2012).
 - [13] D. Liu, W. Zhang, D. Mou, J. He, Y.-B. Ou, Q.-Y. Wang, Z. Li, L. Wang, L. Zhao, S. He, Y. Peng, X. Liu, C. C. Chen, L. Yu, G. Liu, X. Dong, J. Zhang, C. C. Chen, Z. Xu, J. Hu, X. Chen, X. Ma, Q. Xue, and X. Zhou, *Nature Communications* **3**, 931 (2012), [arXiv:1202.5849](#).
 - [14] S. He, J. He, W. Zhang, L. Zhao, D. Liu, X. Liu, D. Mou, Y.-B. Ou, Q.-Y. Wang, Z. Li, L. Wang, Y. Peng, Y. Liu, C. Chen, L. Yu, G. Liu, X. Dong, J. Zhang, C. Chen, Z. Xu, X. Chen, X. Ma, Q. Xue, and X. J. Zhou, *Nature Materials* **12**, 605 (2013).
 - [15] J. J. Lee, F. T. Schmitt, R. G. Moore, S. Johnston, Y.-T. Cui, W. Li, M. Yi, Z. K. Liu, M. Hashimoto, Y. Zhang, D. H. Lu, T. P. Devereaux, D.-H. Lee, and Z.-X. Shen, *Nature* **515**, 245 (2014).
 - [16] P. Zhang, X. L. Peng, T. Qian, P. Richard, X. Shi, J. Z. Ma, B. B. Fu, Y. L. Guo, Z. Q. Han, S. C. Wang, L. L. Wang, Q. K. Xue, J. P. Hu, Y. J. Sun, and H. Ding, (2015), [arXiv:1512.01949](#).
 - [17] G. Zhou, D. Zhang, C. Liu, C. Tang, X. Wang, Z. Li, C. Song, S. Ji, K. He, L. Wang, X. Ma, and Q.-K. Xue, (2015), [arXiv:1512.01948](#).
 - [18] R. Peng, H. C. Xu, S. Y. Tan, H. Y. Cao, M. Xia, X. P. Shen, Z. C. Huang, C. H. P. Wen, Q. Song, T. Zhang, B. P. Xie, X. G. Gong, and D. L. Feng, *Nature communications* **5**, 5044 (2014).
 - [19] F.-C. Hsu, J.-Y. Luo, K.-W. Yeh, T.-K. Chen, T.-W. Huang, P. M. Wu, Y.-C. Lee, Y.-L. Huang, Y.-Y. Chu, D.-C. Yan, and M.-K. Wu, *Proceedings of the National Academy of Sciences* **105**, 14262 (2008).
 - [20] S. Medvedev, T. M. McQueen, I. a. Troyan, T. Palasyuk, M. I. Erements, R. J. Cava, S. Naghavi, F. Casper, V. Ksenofontov, G. Wortmann, and C. Felser, *Nature materials* **8**, 630 (2009), [arXiv:0903.2143](#).
 - [21] S. Tan, Y. Zhang, M. Xia, Z. Ye, F. Chen, X. Xie, R. Peng, D. Xu, Q. Fan, H. Xu, J. Jiang, T. Zhang, X. Lai, T. Xiang, J. Hu, B. Xie, and D. Feng, *Nature Materials* **12**, 634 (2013).
 - [22] X. Liu, L. Zhao, S. He, J. He, D. Liu, D. Mou, B. Shen, Y. Hu, J. Huang, and X. J. Zhou, *Journal of Physics: Condensed Matter* **27**, 183201 (2015).
 - [23] X. Liu, D. Liu, W. Zhang, J. He, L. Zhao, S. He, D. Mou, F. Li, C. Tang, Z. Li, L. Wang, Y. Peng, Y. Liu, C. Chen, L. Yu, G. Liu, X. Dong, J. Zhang, C. Chen, Z. Xu, X. Chen, X. Ma, Q. Xue, and X. J. Zhou, *Nature Communications* **5**, 5047 (2014).
 - [24] L. Rademaker, Y. Wang, T. Berlijn, and S. Johnston, *New Journal of Physics* **18**, 022001 (2016).
 - [25] Y. Wang, K. Nakatsukasa, L. Rademaker, T. Berlijn, and S. Johnston, (2016), [arXiv:1602.00656](#).
 - [26] Z.-X. Li, F. Wang, H. Yao, and D.-H. Lee, , 5 (2015), [arXiv:1512.06179](#).
 - [27] Y. Miyata, K. Nakayama, K. Sugawara, T. Sato, and T. Takahashi, *Nature Materials* **14**, 775 (2015).
 - [28] X. Chen, S. Maiti, A. Linscheid, and P. J. Hirschfeld, *Physical Review B* **92**, 224514 (2015).
 - [29] K. Liu, Z.-Y. Lu, and T. Xiang, *Physical Review B* **85**, 235123 (2012).
 - [30] N. F. Berk and J. R. Schrieffer, *Physical Review Letters* **17**, 433 (1966).
 - [31] N. E. Bickers, D. J. Scalapino, and S. R. White, *Phys. Rev. Lett.* **62**, 961 (1989).
 - [32] S. Graser, T. A. Maier, P. J. Hirschfeld, and D. J. Scalapino, *New Journal of Physics* **11**, 025016 (2009), [arXiv:0812.0343](#).
 - [33] F. Essenberg, A. Sanna, A. Linscheid, F. Tondetzy, G. Profeta, P. Cudazzo, and E. K. U. Gross, *Physical Review B* **90**, 214504 (2014).
 - [34] P. B. Allen and R. C. Dynes, *Physical Review B* **12**, 905 (1975).
 - [35] Y. Fang, D. H. Xie, W. Zhang, F. Chen, W. Feng, B. P. Xie, D. L. Feng, X. C. Lai, and S. Y. Tan, , 8 (2015), [arXiv:1511.05418](#).